Comparison between numerical and analytical results on the required rf current for stabilizing neoclassical tearing modes

Xiaojing Wang[1,2], Qingquan Yu[3,*], Xiaodong Zhang[2,*], Yang Zhang[2], Sizheng Zhu[2], Xiaoguang Wang[2], Bin Wu[2]

[1]University of Science and Technology of China, Hefei, China

[2]Institute of Plasma Physics, Chinese Academy of Sciences, Hefei, China

[3]Max-Planck-Institut für Plasmaphysik, D-85748, Garching, Germany

Abstract

Numerical studies on the stabilization of neoclassical tearing modes (NTMs) by electron cyclotron current drive (ECCD) have been carried out based on reduced MHD equations, focusing on the amount of the required driven current for mode stabilization and the comparison with analytical results. The dependence of the minimum driven current required for NTM stabilization on some parameters, including the bootstrap current density, radial width of the driven current, radial deviation of the driven current from the resonant surface, and the island width when applying ECCD, are studied. By fitting the numerical results, simple expressions for these dependences are obtained. Analysis based on the modified Rutherford equation (MRE) has also been carried out, and the corresponding results have the same trend as numerical ones, while a quantitative difference between them exists. This difference becomes smaller when the applied radio frequency (rf) current is smaller.

Keywords: neoclassical tearing mode (NTM); electron cyclotron current drive (ECCD); rf current; reduced MHD equations; modified Rutherford equation (MRE).

*E-mail: xdzhang@ipp.ac.cn and qiy@ipp.mpg.de

1. Introduction

The neoclassical tearing modes (NTMs), driven by the bootstrap current perturbation due to the flattening of plasma pressure inside a magnetic island [1-3], are often observed in tokamak experiments [4-11]. They are found to degrade the plasma energy confinement, limiting the achievable plasma β value below that predicted by ideal MHD theory [3, 5, 8, 9, 11-15]. Therefore, NTMs have to be stabilized for a fusion reactor.

It is well known that NTMs can be suppressed by localized radio frequency (rf) current drive, with the driven current in the direction along the plasma current to compensate the missing bootstrap current inside the island [10-13, 16-18]. The electron cyclotron wave (ECW) has a good localization of power deposition because of its narrow beams and strong absorption, so that electron cyclotron current drive (ECCD) is suitable for NTM stabilization. The stabilization of NTMs by ECCD has been carried out in tokamak experiments, e.g. on ASDEX-U, DIII-D, JT-60U, TCV [9-11, 15, 16, 19-21]. For ITER it is proposed to utilize 20 MW of ECW power at 170 GHz from a relatively high launching position to control the $m/n = 3/2$ (m and n are the poloidal and toroidal mode numbers) and $2/1$ NTMs [22]. A cross-machine benchmark using the modified Rutherford equation (MRE) has been made, suggesting that 20 MW of ECW power with a normalized (to plasma minor radius) driven current width 0.05 will be sufficient in greatly reducing the amplitude of the $m/n = 3/2$ and $2/1$ NTMs for a local bootstrap current density fraction 0.16 in ITER [23].

Theoretically, there are three kinds of approaches on the NTM stabilization by ECCD. One is based on the analysis of the MRE [3, 8, 23, 24], the second one is based on the numerical simulation of reduced MHD equations [12-14], and the third one is based on the extended MHD equations derived from the kinetic equation including the rf source [25-27]. Numerical effort based on the third method is still ongoing. Most existing studies are based on the MRE, for which the value of the tearing mode stability index has to be assumed and is subject to certain level of uncertainty, since the tearing mode stability index in the nonlinear phase is different from the linear one. The second approach is more complicated and takes long computation time, but the change of the plasma current density profile is self-consistently included, and the tearing mode stability index is not needed. It is of great interest in learning the difference between the results obtained from these two approaches. In addition, for the design of a fusion reactor it is important to know the dependence of the required driven current for NTM stabilization on the plasma and rf current parameters.

In this paper, the stabilization of NTMs by ECCD is studied numerically following the second kind approach for both the modulated current drive (MCD) phased with the island's O-point and the continuous or non-modulated current drive (NMCD). The dependence of the minimum required driven current for NTM stabilization on some parameters is calculated, including the bootstrap current density, radial ECW deposition width, the island width when applying ECW, and the radial deviation of the rf current from the resonant surface. By fitting the numerical results, simple expressions are obtained for these dependences. In addition, analysis based on the MRE has also been carried out to compare with numerical results, showing that they qualitatively agree each other, while a quantitative difference between them exists.

Our numerical calculation model is described in section 2, followed by the numerical results in section 3. The comparison between numerical results and those from the MRE is presented in Section 4. The discussion and summary are in section 5.

2. Numerical calculation model

Periodical cylindrical geometry is utilized, and the magnetic field $\boldsymbol{B}$ is defined to be

$$\boldsymbol{B} = B_{0t}\boldsymbol{e_t} - (nr/mR)B_{0t}\boldsymbol{e_\theta} + \nabla\psi \times \boldsymbol{e_t}, \quad (1)$$

where ψ is the helical flux function, m/r and n/R are the wave vectors in $\boldsymbol{e_\theta}$ (poloidal) and $\boldsymbol{e_t}$ (toroidal) direction, respectively, R is the major radius, and B_{0t} is the toloidal equilibrium magnetic field.

The Ohm's law, the plasma vorticity equation and the plasma pressure evolution equation are utilized,

$$\frac{\partial\psi}{\partial t} + \boldsymbol{v}\cdot\nabla\psi = E - \eta\left(j_p - j_b - j_d\right), \quad (2)$$

$$\rho\left(\frac{\partial}{\partial t} + \boldsymbol{v}\cdot\nabla\right)\nabla^2\emptyset = \boldsymbol{e_t}\cdot(\nabla\psi\times\nabla j_p) + \rho\mu\nabla^4\emptyset, \quad (3)$$

$$\frac{3}{2}\left(\frac{\partial}{\partial t} + \boldsymbol{v}\cdot\nabla\right)p = \nabla\cdot(\chi_\parallel\nabla_\parallel p) + \nabla\cdot(\chi_\perp\nabla_\perp p) + Q, \quad (4)$$

where $\boldsymbol{v} = \nabla\emptyset\times\boldsymbol{e_t}$, $\emptyset$ is the stream function. $j_p = -\nabla^2\psi - 2nB_{0t}/(mR)$, $j_b = -c_b\frac{\sqrt{\varepsilon}}{B_\theta}p'$ [1-3] and j_d are the plasma current density, the bootstrap current density, and the driven current density by ECW in the $\boldsymbol{e_t}$ direction, respectively. The prime denotes the radial derivative. ρ is the plasma mass density, η the plasma resistivity, μ the plasma viscosity, p the plasma pressure, $\nabla_\parallel$ and $\nabla_\perp$ are the parallel and perpendicular gradient. $\chi_\parallel$ and $\chi_\perp$ are the parallel and perpendicular heat transport coefficients, and Q and E are the heating power and the equilibrium electric field, respectively. c_b is a constant of the order of unity, $\varepsilon = r/R$ the inverse aspect ratio, and B_θ the poloidal magnetic field. The plasma density and ion temperature are assumed to be constant for simplicity.

The driven current density by ECW is assumed to be proportional to the fast electron density n_f, which is calculated from [12]

$$\frac{\partial n_f}{\partial t} = \nabla\cdot\left(\chi_{\parallel f}\nabla_\parallel n_f\right) + \nabla\cdot\left(\chi_{\perp f}\nabla_\perp n_f\right) + \nu_f(n_{fs} - n_f), \quad (5)$$

where $\chi_{\parallel f}$ ($\chi_{\perp f}$) is the parallel (perpendicular) transport coefficient, $1/\nu_f$ is the slowing-down time of the fast electrons. The fast electron source density generated by ECW, n_{fs}, is defined by [12, 17]

$$n_{fs} = n_{fs0}\exp[-\left(\frac{r-r_{cd}}{w_{cd}}\right)^2]\Pi(h_0, \Delta h), \quad (6)$$

where n_{fs0}, w_{cd} and r_{cd} are the amplitude, the half width and the radial deposition location of the source, respectively. The square box function $\Pi(h_0, \Delta h)$ is equal to 1 for $|h - h_0| < \Delta h$ and to 0 otherwise, defining the helical angle of the ECW deposition, where $h_0 = \omega t$, ω is the relative rotation frequency between the mode and the ECW deposition, and Δh is the instantaneous wave deposition width along the helical angle $h = m\theta + n\xi$. The magnetic island is assumed to be not rotating, while the ECW deposition rotates along the helical angle with respect to the island.

Because the cylindrical geometry is utilized here, the toroidal effect, such as the Glasser effect [28, 29], is neglected. In addition, the diamagnetic drift and the associated ion polarization current [30-35] have not been included. It is known that the Glasser effect and the ion polarization current are important for the stability of a small island. Once the island is sufficiently large, however, they become negligible compared to the bootstrap current perturbation for the island growth. Therefore, our model is valid for a large island but is inaccurate for a sufficiently small island when the Glasser effect and the ion polarization current are important.

Normalized quantities are used in our calculations. The time t is normalized to τ_R, the length to

a, the helical flux to aB_{0t}, current density to $B_{0t}/\mu_0 a$, and the transport coefficients to a^2/τ_R, where $\tau_R = a^2\mu_0/\eta$ is the resistive time and a is the minor radius. The viscous time $\tau_\mu = a^2/\mu$ is assumed to be ten times smaller than the resistive time.

3. Numerical results

In Section 3.1 the numerical results on the parameters affecting NTM stabilization by ECCD are shown. The minimum driven current required for fully stabilizing the NTM is presented in Section 3.2.

3.1 Parameters affecting NTM stabilization by ECCD

The input parameters of our numerical calculations are as the following if not mentioned elsewhere: ECCD is applied at the resonant surface with $w_{cd}/a = 0.05$, $\Delta h = 0.482$, $\omega = 3\times10^4/\tau_R$, $\nu_f = 3\times10^3/\tau_R$, $\chi_\perp = \chi_{\perp f} = 13.0a^2/\tau_R$ and $\chi_\parallel/\chi_\perp = \chi_{\parallel f}/\chi_{\perp f} = 10^8$. The Lundquist number $S = \tau_R/\tau_A$ is taken to be 1.0×10^8, where τ_A is the Alfvén time. A monotonic radial profile for the safety factor q is utilized, with the local magnetic shear length $L_q = \frac{q}{q'}|_{r=r_s}$=$0.41a$ at the $q = 1.5$ surface, and $r_s = 0.555a$ is the minor radius of the $q = 1.5$ surface. The local bootstrap current density fraction at the resonant surface $j_b/j_p = 0.173$ is taken. The inverse aspect ratio $\varepsilon = a/R$ is taken to be 0.28.

An example of the time evolution of the normalized $m/n = 3/2$ magnetic island width, w/a, is shown in figure 1. The solid curve is for the case without applying ECCD. Driven by the bootstrap current perturbation, the island grows up in a time scale about $0.01\tau_R$. After nonlinear mode saturation, ECW is turned on at $t/\tau_R = 0.04$ with $I_{cd}/I_p = 0.02$, where I_{cd} is the driven current by ECW, and I_p is the plasma current. The dashed curve is for the case of MCD phased with the island's O-point (50% duty cycle), and the dot-dashed curve is for NMCD. MCD has a slightly stronger stabilization effect than NMCD does in this case.

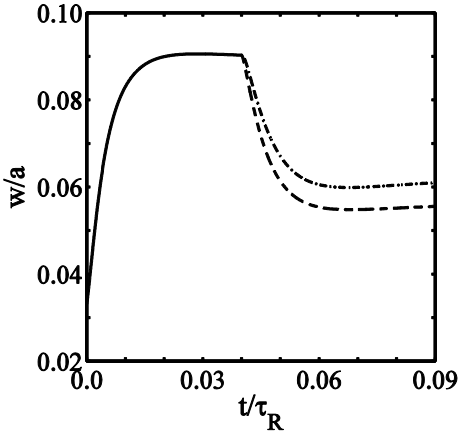

Figure 1. Time evolution of the normalized $m/n = 3/2$ island width w/a without ECCD (solid curve). The dashed (dot-dashed) curve is for MCD (NMCD) with $I_{cd}/I_p = 0.02$.

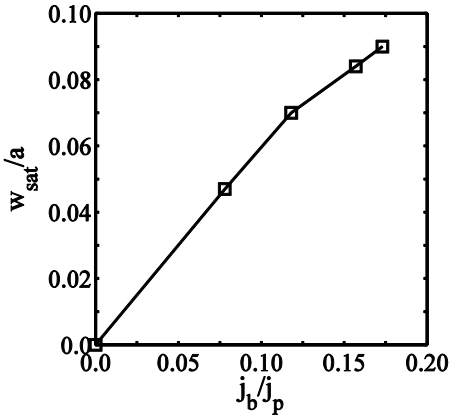

Figure 2. Normalized saturated 3/2 island width w_{sat}/a versus the local bootstrap current density fraction j_b/j_p without applying ECCD.

Without applying ECCD, the $m/n = 3/2$ magnetic island width at nonlinear saturation is shown in figure 2 as a function of the local bootstrap current density fraction j_b/j_p, obtained by varying the plasma beta value while keeping other input parameters unchanged in calculations. The saturated island width is approximately proportional to local equilibrium bootstrap current density. This is as expected from the MRE [2, 3],

$$\frac{\tau_r}{r_s}\frac{dw}{dt} = \Delta_0' r_s + \Delta_b' r_s - \Delta_{cd}' r_s, \tag{7}$$

in which $\tau_r = \frac{\mu_0 r_s^2}{1.22\eta}$. Δ_0' is the tearing mode stability index, $\Delta_b' = 4.6\sqrt{\varepsilon}\frac{2\mu_0(-p')}{B_\theta^2} L_q \frac{w}{w^2+w_d^2}$ is the bootstrap current perturbation term, Δ_{cd}' is the driven current term, and w_d is the characteristic island width above which the plasma pressure is flattened across the island [2]. Without ECCD, the saturated island width (for $w \gg w_d$) is proportional to the local radial gradient of the pressure or the local bootstrap current density.

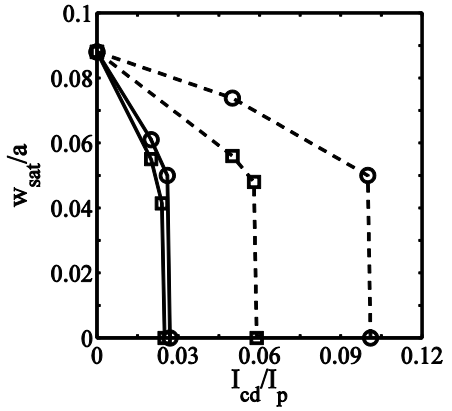

Figure 3. Normalized saturated island width w_{sat}/a for the 3/2 mode versus the driven current fraction I_{cd}/I_p for $w_{cd}/a = 0.05$ (solid curve) and 0.10 (dashed). The square (circle) symbols are for MCD (NMCD).

The saturated magnetic island width for the 3/2 mode is shown in figure 3 as a function of the

driven current fraction I_{cd}/I_p for different ECW deposition width, $w_{cd}/a = 0.05$ (solid curve) and 0.10 (dashed). The square (circle) symbols are for MCD (NMCD). The stabilizing effect of ECCD for a smaller w_{cd} is stronger than that for a large one, since the driven current density is larger in this case for the same amount of driven current. MCD and NMCD have nearly the same stabilizing effect for a small w_{cd}, while NMCD is less effective than MCD for a large w_{cd}, as expected [13, 15]. In addition, the saturated island width decreases linearly with the driven current amplitude when the rf current is sufficiently small. When a critical driven current is reached, the island width decreases to zero rapidly, because the island width is close to the characteristic island width w_d, which equals $0.0437a$ for our input parameters [2]. The critical driven current is the minimum driven current required for NTM stabilization.

In addition to the $m/n = 3/2$ NTMs, the $m/n = 2/1$ modes can also grow to a large amplitude [36-40] and sometimes even cause plasma major disruptions. The stabilization of the $3/2$ and the $2/1$ modes by ECCD is compared in the following. Without applying ECCD, the time evolution of (a) the tearing mode stability index $\Delta_0' r_s$ and (b) the island width are shown in figure 4, where the solid and dashed curves are for the $3/2$ mode ($j_b = 2.13 \times 10^{-2}\ in\ the\ unit\ of\ B_{0t}/\mu_0 a$ at $r_{3/2} = 0.555a$ [2]) and the $2/1$ mode ($j_b = 1.07 \times 10^{-2}\ in\ the\ unit\ of\ B_{0t}/\mu_0 a$ at $r_{2/1} = 0.673a$), respectively. The same safety factor profile is used for these two modes. The values of Δ_0' is calculated from [40, 41]

$$\Delta_0' = \frac{\psi_1'(r_+) - \psi_1'(r_-)}{\psi_1(r_s)}, \tag{8}$$

where ψ_1 is the perturbed helical flux function of the $m/n = 3/2$ or 2/1 component, and r_+ and r_- are the minor radius of the outer and the inner edges of the island obtained from numerical calculations. It is seen that the $2/1$ mode grows to a larger amplitude than the $3/2$ mode does. According to equation (7), the saturated island width without ECCD is given by

$$w_{sat} \approx \frac{1}{-\Delta_0' r_s} 4.6\sqrt{\varepsilon}\, \frac{2\mu_0(-p')}{B_\theta^2} L_q r_s. \tag{9}$$

A less negative value of $\Delta_0' r_s$ for the 2/1 mode leads to a larger saturated island.

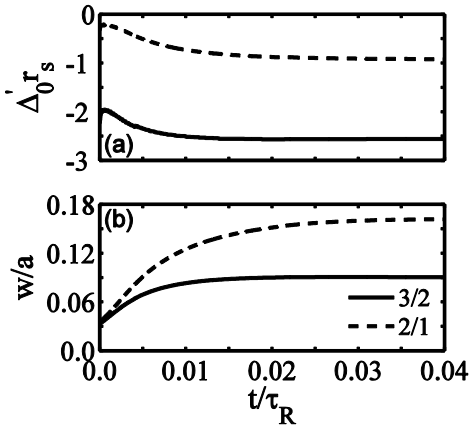

Figure 4. Time evolution of (a) $\Delta_0' r_s$ and (b) normalized island width without ECCD. The solid and dashed curves are for $3/2$ and the $2/1$ mode, respectively.

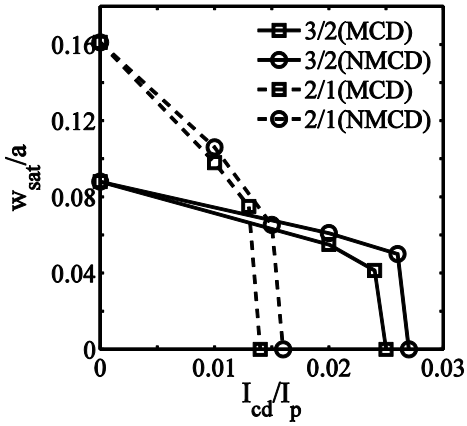

Figure 5. Normalized saturated island width w_{sat}/a versus I_{cd}/I_p for the $3/2$ (solid curves) and $2/1$ NTMs (dashed) with $w_{cd}/a = 0.05$. The square (circle) symbols are for MCD (NMCD).

Corresponding to figure 4, the saturated island width is shown as a function of I_{cd}/I_p in figure 5 for the $3/2$ (solid curves) and $2/1$ NTMs (dashed) with $w_{cd}/a = 0.05$. The square (circle) symbols are for MCD (NMCD). The required driven current for fully stabilizing the $2/1$ mode is less than that for stabilizing the $3/2$ mode. The bootstrap current density is smaller at the $q = 2/1$ surface than that at the $3/2$ surface for the above case. Therefore, a smaller rf current is required to compensate the missing bootstrap current inside an island. Above results indicate that the required driven current for NTM stabilization depends more on the local bootstrap current density than on the value of the $\Delta_0' r_s$, if the bootstrap current density is not too low.

For above results the ECCD is applied right at the resonant surface. The radial misalignment between ECW deposition and the resonant surface significantly affects the NTM stabilization. For $w_{cd}/a = 0.05$ and $j_b/j_p = 0.173$, the saturated 3/2 island width for MCD is shown in figure 6 as a function of the normalized radial deviation of ECW deposition from the rational surface, $x = \frac{r_{cd} - r_s}{a}$, for $I_{cd}/I_p = 0.03$ (solid curve) and 0.02 (dashed). A sufficiently large shift of ECW deposition away from the rational surface can significantly decrease the stabilizing efficiency as expected.

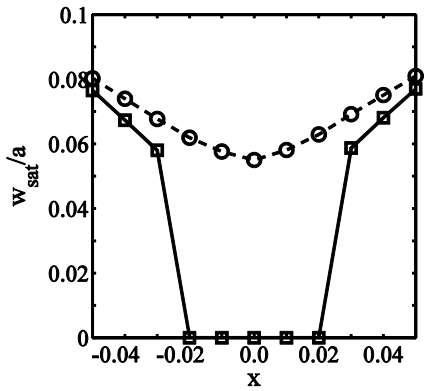

Figure 6. Normalized saturated 3/2 island width for MCD versus the normalized radial deviation of the rf current, $x = \frac{r_{cd} - r_s}{a}$, for $I_{cd}/I_p = 0.03$ (solid curve) and 0.02 (dashed) with $w_{cd}/a = 0.05$.

3.2 The minimum rf current required for NTM stabilization

In order to obtain the minimum rf current required for fully stabilizing the $3/2$ NTM, $I_{cd,r}$, numerical calculations have been carried out to scan over the driven current amplitude similar to that shown in figure 3. With $w_{cd}/a = 0.05$, $I_{cd,r}/I_p$ is shown as a function of the local bootstrap current density fraction j_b/j_p in figure 7 for MCD (square symbols) and NMCD (circle). It is seen that $I_{cd,r}$ depends linearly on j_b/j_p for both cases. The polynomial fitting to the numerical results leads to the relations

$$\frac{I_{cd,r}}{I_p} = 0.2399\frac{j_b}{j_p} - 0.0166 \tag{10}$$

for MCD and

$$\frac{I_{cd,r}}{I_p} = 0.2534\frac{j_b}{j_p} - 0.0168 \tag{11}$$

for NMCD, which are also shown in figure 7 by the solid and dashed curves.

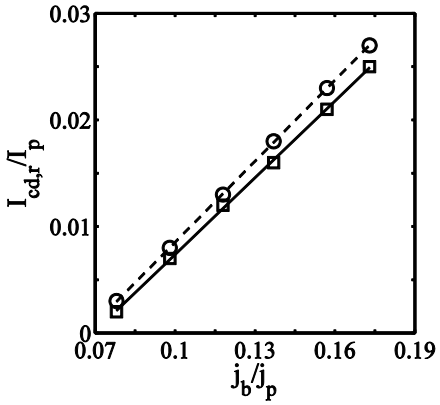

Figure 7. The minimal driven current required for 3/2 NTM stabilization (normalized to plasma current I_p), $I_{cd,r}/I_p$, versus the local j_b/j_p at the resonant surface for $w_{cd}/a = 0.05$. The square (circle) symbols are the numerical results for MCD (NMCD), and the solid and dashed curves are the fitting results from equations (10) and (11).

In figure 8 $I_{cd,r}/I_p$ for the 3/2 mode is shown as a function of the half width of driven current w_{cd} with $j_b/j_p = 0.173$ at the resonant surface for MCD (square symbols) and NMCD (circle). It is proportional to w_{cd} for MCD but approximately to the square of w_{cd} for NMCD. Fitting of the numerical results leads to

$$\frac{I_{cd,r}}{I_p} = 0.6571\frac{w_{cd}}{a} - 0.0072 \tag{12}$$

for MCD and

$$\frac{I_{cd,r}}{I_p} = 11.6071\left(\frac{w_{cd}}{a}\right)^2 - 0.2601\frac{w_{cd}}{a} + 0.0106 \tag{13}$$

for NMCD, which are also shown in figure 8 by the solid and dashed curves.

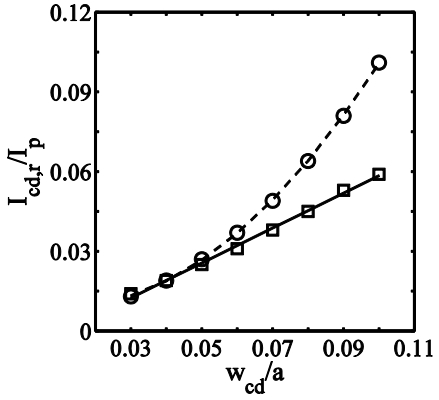

Figure 8. $I_{cd,r}/I_p$ for the 3/2 mode versus w_{cd} for $j_b/j_p = 0.173$ at the resonant surface. The square (circle) symbols are the numerical results for MCD (NMCD), and the solid and dashed curves are the fitting results from equations (12) and (13).

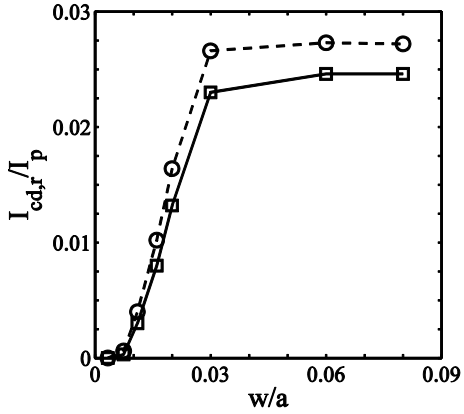

Figure 9. $I_{cd,r}/I_p$ for the 3/2 mode versus the normalized island width for MCD (solid curve) and NMCD (dashed), with $w_{cd}/a = 0.05$ and $j_b/j_p = 0.173$ at the resonant surface. ECCD is applied when the island width grows to the value shown by the horizontal axis.

When ECCD is applied during the island growth before nonlinear saturation, less driven current is expected to be required for mode stabilization. In figure 9 $I_{cd,r}/I_p$ for the 3/2 mode is shown as a function of the normalized island width w/a for MCD (solid curve) and NMCD (dashed), with $w_{cd}/a = 0.05$ and $j_b/j_p = 0.173$ at the resonant surface. ECCD is applied when the island width grows to the value shown by the horizontal axis. It is seen that before mode saturation, the required driven current for mode stabilization scales linearly with w for both MCD and NMCD due to the finite w_d and a larger stabilizing effect of ECCD for a smaller island, indicating the advantage of applying ECCD earlier. The pressure evolution equation (equation (4)) takes into account both the parallel and the perpendicular transport, so that the numerical results are affected by the ratio between them, which is equivalent the effect of w_d in the MRE [2].

The radial misalignment between ECW deposition and the resonant surface decreases the stabilizing effect, as seen from figure 6. With $w_{cd}/a = 0.05$ and $j_b/j_p = 0.173$ at the resonant surface, $I_{cd,r}/I_p$ for the 3/2 mode is shown in figure 10 as a function of the radial deviation of the rf current, x, for MCD (square symbols) and NMCD (circle). ECCD is applied after nonlinear mode

saturation. $I_{cd,r}/I_p$ significantly increases if the radial deviation $x > 0.02$, especially for NMCD. ECCD deposited at the outer side of the rational surface is better than that at the inner side in agreement with experimental observations [4, 42, 43], since a larger current density gradient around the inner edge of the island is destabilizing [44, 45].

The polynomial fitting to the numerical results shows the relation

$$\frac{I_{cd,r}}{I_p} = 23.0844x^2 - 0.0883x + 0.0223 \tag{14}$$

for MCD and

$$\frac{I_{cd,r}}{I_p} = 50.0106x^2 - 0.4895x + 0.0225 \tag{15}$$

for NMCD, which are shown by the solid and dashed curves in figure 10, respectively.

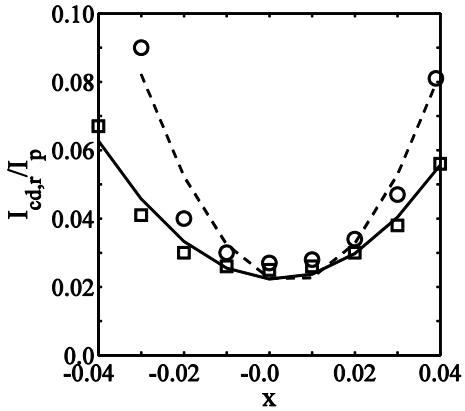

Figure 10. $I_{cd,r}/I_p$ for the 3/2 mode versus the normalized radial deviation of the rf current x, with $w_{cd}/a = 0.05$ and $j_b/j_p = 0.173$ at the resonant surface. The square (circle) symbols are the numerical results for MCD (NMCD), and the solid and dashed curves are the fitting results. ECCD is applied after nonlinear mode saturation.

4. Comparison between numerical results and MRE

The driven current term in equation (7) has the following form [2, 3],

$$\Delta'_{cd} = \frac{16}{\pi}\frac{\mu_0 I_{cd} L_q}{r_s B_\theta}\frac{1}{(2w_{cd})^2}\eta_{cd}, \tag{16}$$

where η_{cd} is the so-called stabilization efficiency. Results obtained from the MRE utilizing equations (7) and (16) are shown in figure 11 for the $m/n = 3/2$ island, where $j_b/j_p = 0.173$, $L_q = 0.41a$ at $r_s = 0.555a$ and $w_{cd}/a = 0.05$ are taken. Δ'_0 is calculated by equation (8). The solid curve is the case without the driven current. It is seen that $\mathrm{d}w/\mathrm{d}t$ is not zero at the saturated island width $0.09a$, as shown in figure 4, indicating that the equation $\Delta'_0 + \Delta'_b = 0$ is not accurate in determining the saturated island width. The dashed and the dot-dashed curves are for MCD with $I_{cd}/I_p = 0.0188$ and for NMCD with $I_{cd}/I_p = 0.0345$, respectively. For these values of I_{cd}/I_p the maximal of dw/dt is zero, i.e., the minimal driven current required for mode stabilization.

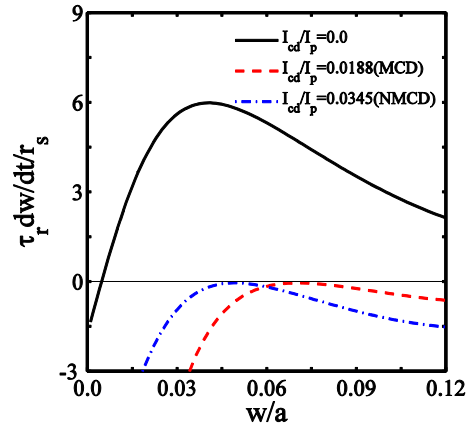

Figure 11. The values of dw/dt obtained from MRE for the $m/n = 3/2$ island with $j_b/j_p = 0.173$, $L_q = 0.41a$ at $r_s = 0.555a$ and $w_{cd}/a = 0.05$. The solid curve is the case without the driven current. The dashed and dot-dashed curves are for MCD with $I_{cd}/I_p = 0.0188$ and for NMCD with $I_{cd}/I_p = 0.0345$, respectively.

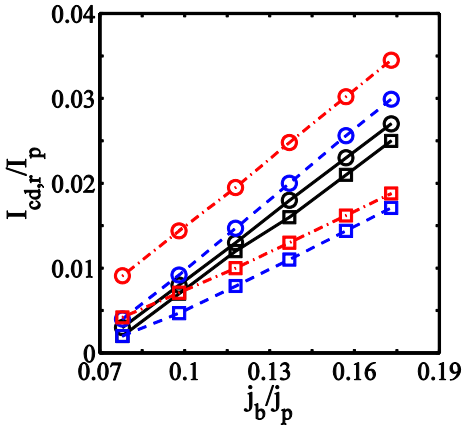

Figure 12. $I_{cd,r}/I_p$ versus j_b/j_p for $w_{cd}/a = 0.05$, obtained numerically (solid curves). The dashed (dot-dashed) curves are obtained from MRE using $\Delta_0' = -m/r_s$ (the Δ_0' calculated by equation (8)). The square (circle) symbols are for MCD (NMCD).

To compare the numerical results with those obtained from the MRE, $I_{cd,r}/I_p$ is shown as a function of the local j_b/j_p at the resonant surface for $w_{cd}/a = 0.05$ in figure 12. The solid curves are obtained from numerical calculations. The dashed curves are obtained from MRE using $\Delta_0' = -m/r_s$. The dot-dashed curves are also obtained from MRE but using the Δ_0' calculated from equation (8). The square (circle) symbols are for MCD (NMCD). The numerical results have the same trend as those from MRE. A quantitative difference between numerical results and those from MRE exists.

Figure 13 shows $I_{cd,r}/I_p$ as a function of the half width of driven current, w_{cd}, with $j_b/j_p = 0.173$ at the resonant surface. Both numerical results and those from MRE reveal an approximately linear relation for MCD but quadratic relation for NMCD between $I_{cd,r}/I_p$ and w_{cd}. The quantitative difference between numerical results and those form MRE is larger for a larger w_{cd} or $I_{cd,r}$.

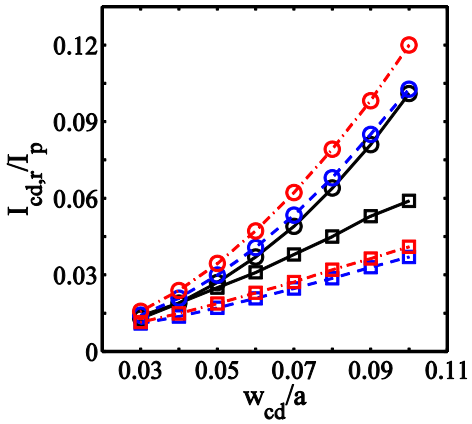

Figure 13. $I_{cd,r}/I_p$ versus w_{cd}/a for $j_b/j_p = 0.173$ obtained numerically (solid curves). The dashed (dot-dashed) curves are obtained from MRE using $\Delta_0' = -m/r_s$ (the Δ_0' calculated by equation (8)). The square (circle) symbols are for MCD (NMCD).

According to equations (7) and (16), the required driven current for mode stabilization is proportional to $y = (\frac{w_{cd}}{a})^2 \frac{1}{\eta_{cd}}$. The parameter y as a function of the full width of driven current is shown in figure 14, where the solid, dashed and dot-dashed curves are for $w/a = 0.01,\ 0.05$ and 0.1, respectively. The black (blue) curves are for MCD (NMCD). There is also a linear (quadratic) relationship between y and w_{cd} with MCD (NMCD), explaining the results shown in figure 13.

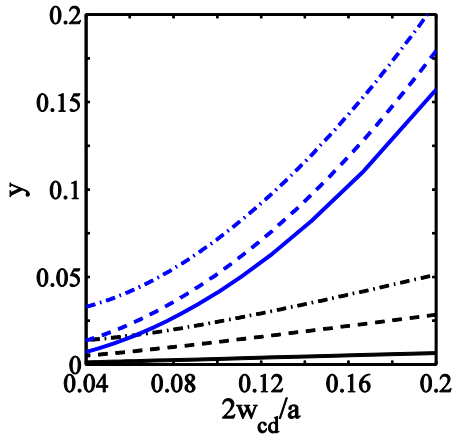

Figure 14. The parameter $y = (\frac{w_{cd}}{a})^2 \frac{1}{\eta_{cd}}$ versus the full width of driven current. The solid, dashed and dot-dashed curves are for $w/a = 0.01,\ 0.05$ and 0.1, respectively. The black (blue) curves are for MCD (NMCD).

$I_{cd,r}/I_p$ is shown as a function of the radial deviation of the rf current x in figure 15. The numerical results have the same trend as those obtained from the MRE. The quantitative difference between them is smaller if the rf current is accurately applied at the resonant surface. In this case $I_{cd,r}$ is smaller. The values of $I_{cd,r}/I_p$ obtained from MRE are symmetric on the two sides of the rational surface, being different from numerical results for which the effect of the plasma current profile is self-

consistently included. It should be mentioned that with NMCD, the obtained value of Δ'_{cd} is negative for $|x| > 0.045a$ due to the destabilizing effect of driven current deposited around the island edge, in agreement with the previous finding [46].

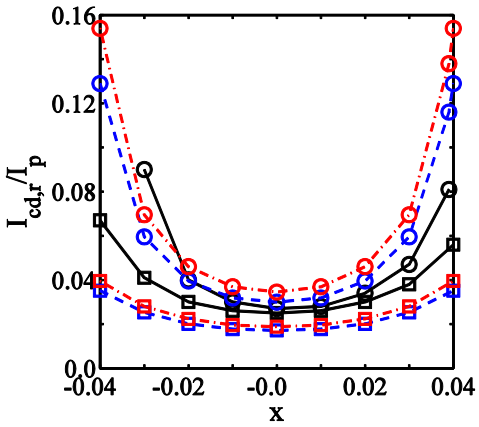

Figure 15. $I_{cd,r}/I_p$ versus the radial deviation of the rf current x, obtained numerically (solid curves). The dashed (dot-dashed) curves are obtained from MRE using $\Delta'_0 = -m/r_s$ (the Δ'_0 calculated by equation (8)). The square (circle) symbols are for MCD (NMCD).

5. Discussion and summary

The stabilization of NTMs by ECCD is theoretically studied in this paper. The numerical results qualitatively agree with those obtained from the MRE. However, there is a quantitative difference between them. The difference becomes larger for a larger driven current width and a larger radial deviation of the rf current from the resonant surface, as shown in figures 13 and 15. In these cases the required driven current for mode stabilization is larger. A possible explanation is that a larger driven current results in a larger change of the local plasma density profile and therefore a larger difference. It is known that the local plasma current density profile is affected by the amplitude, width and the radial location of the rf current. It is interesting to note that when the rf current is accurately applied at the resonant surface with a smaller w_{cd} such that the required driven current for NTM stabilization is smaller, the difference between numerical results and those from the MRE is smaller, and the MRE gives a good approximation.

The required rf current for mode stabilization is affected by the bootstrap current fraction, the driven current width, the turn-on time of ECCD, the ECW deposition location, as well as the way of current drive, MCD or NMCD. Linear relations are found between the required rf current and j_b/j_p for both MCD and NMCD, as expected. There is an approximately linear relationship between $I_{cd,r}/I_p$ and w_{cd} for MCD but a quadratic relationship for NMCD, indicating the benefit of MCD for a large driven current width. When ECCD is applied during the island growth, the required driven current for mode stabilization linearly increases with island width for both MCD and NMCD, implying the advantage of applying ECCD earlier. When there is a radial deviation of the rf current from the island, $I_{cd,r}/I_p$ for mode stabilization significant increases, especially for NMCD, showing the importance of an accurate ECW deposition.

The simple polynomial relations obtained in the subsection 3.2 can be used to estimate the required rf power for mode stabilization. For ITER with a current drive efficiency $\gamma = nR\frac{I_{cd}}{P_{EC}} = 0.28 \times 10^{19} A/(m^2 \cdot W)$ [47, 48], the plasma density $n = 10^{20}\ m^{-3}$, and the major radius $R = 6.2m$, where

P_{EC} is the ECW power, the required ECW power for mode stabilization, $P_{EC,r}$, as a function of w_{cd} is translated from equations (12)-(13) into

$$\frac{P_{EC,r}}{I_p} = 145.5102\frac{w_{cd}}{a} - 1.5974(\mathrm{MW/MA}) \quad (17)$$

for MCD and

$$\frac{P_{EC,r}}{I_p} = 10^3 \times [2.5702(\frac{w_{cd}}{a})^2 - 0.0576\frac{w_{cd}}{a} + 0.0024](\mathrm{MW/MA}) \quad (18)$$

for NMCD with $j_b/j_p = 0.173$.

Equations (12)-(13) are obtained by fitting the numerical results with w_{cd}/a in the range from 0.03 to 0.1. By fitting of our additional numerical results for a smaller w_{cd}/a, $w_{cd}/a = 0.02$, and zero radial mis-alignment, it is found that $P_{EC,r}/I_p$ has the following dependence on j_b/j_p,

$$\frac{P_{EC,r}}{I_p} = 17.8252\frac{j_b}{j_p} - 1.2349(\mathrm{MW/MA}) \quad (19)$$

for ITER parameters with NMCD.

Using equation (17), the required modulated ECW power for NTM stabilization in ITER is found to be 28 MW for $j_b/j_p = 0.16$, $w_{cd} = 0.025a$ and $I_p = 15MA$, when ECCD is applied after mode saturation without radial mis-alignment. For $w_{cd} = 0.02a$, the required non-modulated ECW power is 24 MW according to equation (19). More ECW power will be required for a larger ECW deposition width or with a radial deviation of the rf current, especially for NMCD with the radial deviation being larger than $0.02a$. However, if ECCD is applied at the right location when the island is still small, the required ECW power will be significantly reduced.

It should be noted that the above value of 28 MW required for the m/n=3/2 NTM stabilization in ITER relies on the ECW deposition width as well as the equilibrium plasma current density profile used for numerical calculations. The required ECW power is lower by about a fact 1.5 obtained from the MRE, depending on the value of Δ_0'. It should also be mentioned that the required power for the m/n=3/2 NTM stabilization in ITER calculated from the MRE in [47] is at the level of 10 MW, because the coefficient for the dependence of the bootstrap current density on the plasma density and temperature gradients is obtained experimentally, which is smaller than that obtained from theories [47, 49].

In summary, theoretical studies on NTM stabilization by ECCD have been carried out to study the dependence of the minimum rf current required for NTM stabilization on some parameters, including the bootstrap current fraction, the radial width of the driven current, the radial deviation of rf current from the rational surface, and the island width when applying ECCD. Simple relations for these dependences are obtained by fitting the numerical results. The results obtained from numerical simulations and from the modified Rutherford equation have the same trend, while there is a quantitative difference between them. When the rf current is accurately applied at the resonant surface with a small ECW deposition width such that the required driven current for NTM stabilization is smaller, the difference between them is smaller.

Acknowledgment

This work was supported by the National Magnetic Confinement Fusion Science Program of China (Contract No. 2012GB103000 and 2012GB103003) and the National Natural Science Foundation of

China (Grant No. 11475225). Numerical computations were performed on the ShenMa High Performance Computing Cluster at the Institute of Plasma Physics, Chinese Academy of Sciences.

References

[1] Carrera R. *et al* 1986 *Phys. Fluids* **29** 899
[2] Fitzpatrick R. 1995 *Phys. Plasmas* **2** 825
[3] Hegna C. C. and Callen J. D. 1997 *Phys. Plasmas* **4** 2940
[4] Hoshino K. *et al* 1992 *Phys. Rev. Lett.* **69** 2208
[5] Sing D. C. *et al* 1993 *Phys. Fluids B* **5** 3239
[6] Kislov D. A. *et al* 1997 *Nucl. Fusion* **37** 339
[7] Westerhof E. *et al* 2007 *Nucl. Fusion* **47** 85
[8] Classen I. G. J. *et al* 2007 *Phys. Rev. Lett.* **98** 035001
[9] Gantenbein G. *et al* 2000 *Phys. Rev. Lett.* **85** 1242
[10] Isayama A. *et al* 2000 *Plasma Phys. Control. Fusion* **42** L37
[11] Zohm H. *et al* 1999 *Nucl. Fusion* **39** 577
[12] Yu Q. *et al* 2000 *Phys. Plasmas* **7** 312
[13] Yu Q. *et al* 2004 *Phys. Plasmas* **11** 1960
[14] Yu Q. and Günter S. 2008 *Nucl. Fusion* **48** 065004
[15] Maraschek M. *et al* 2007 *Phys. Rev. Lett.* **98** 025005
[16] La Haye R. J. 2006 *Phys. Plasmas* **13** 055501
[17] Giruzzi G. *et al* 1999 *Nucl. Fusion* **39** 107
[18] Perkins F. W. *et al*, in *Proceedings of the 24th EPS Conference on Controlled Fusion and Plasma Physics* (European Physical Society), 9-13 June 1997, Berchtesgaden, Germany, Vol. 3, p. 1017
[19] La Haye R. J. *et al* 2002 *Phys. Plasmas* **9** 2051
[20] Felici F. *et al* 2012 *Nucl. Fusion* **52** 074001
[21] Maraschek M. 2012 *Nucl. Fusion* **52** 074007
[22] Hender T. C. *et al* 2007 *Nucl. Fusion* **47** S128
[23] La Haye R. J. *et al* 2006 *Nucl. Fusion* **46** 451
[24] Sauter O. 2004 *Phys. Plasmas* **11** 4808
[25] Hegna C. and Callen J. 2009 *Phys. Plasmas* **16** 112501
[26] Ramos J. 2010 *Phys. Plasmas* **17** 082502
[27] Ramos J. 2011 *Phys. Plasmas* **18** 102506
[28] Glasser A. *et al* 1976 *Phys. Fluids* **19** 567
[29] Lütjens H. *et al* 2001 *Phys. Plasmas* **8** 4267
[30] Smolyakov A. 1993 *Plasma Phys. Control. Fusion* **35** 657
[31] Wilson H. R. *et al* 1996 *Phys. Plasmas* **3** 248
[32] Waelbroeck F. *et al* 2001 *Phys. Rev. Lett.* **87** 215003
[33] Connor J. *et al* 2001 *Phys. Plasmas* **8** 2835
[34] Fitzpatrick R. *et al* 2006 *Phys. Plasmas* **13** 122507
[35] Yu Q. 2010 *Nucl. Fusion* **50** 025014
[36] White R. B. *et al* 1977 *Phys. Rev. Lett.* **39** 1618
[37] Holmes J. A. *et al* 1979 *Nucl. Fusion* **19** 1333
[38] Esposito B. *et al* 2011 *Nucl. Fusion* **51** 083051
[39] Petty C. C. *et al* 2004 *Nucl. Fusion* **44** 243

[40] White R. B. 1986 *Rev. Mod. Phys.* **58** 183
[41] Furth H. P. *et al* 1963 *Phys. Fluids* **6** 459
[42] Esposito B. *et al* 2011 *Plasma Phys. Control. Fusion* **53** 124035
[43] Esposito B. *et al* 2009 *Nucl. Fusion* **49** 065014
[44] Westerhof E. 1987 *Nucl. Fusion* **27** 1929
[45] Westerhof E. 1990 *Nucl. Fusion* **30** 1143
[46] Pletzer A. and Perkins F. W. 1999 *Phys. Plasmas* **6** 1589
[47] Hayashi N. *et al* 2004 *Nucl. Fusion* **44** 477
[48] Wesson J., *Tokamaks*, 3rd ed. (Oxford University Press), 2004
[49] Sauter O. *et al* 1997 *Phys. Plasmas* **4** 1654